Title
Anatomy of a turbulent patch in a large shallow lake

Journal
International Symposium on Stratified Flows, 1(1)

Authors
Boegman, Leon
Bouffard, Damien

Publication Date
2016-08-29

Anatomy of a turbulent patch in a large shallow lake

Leon Boegman, Environmental Fluid Dynamics Lab, Dept of Civil Engineering, Queen's University, K7L 3N6, Canada
Damien Bouffard, Physics of Aquatic Systems Laboratory, EPFL, CH-1015, Lausanne, Switzerland

Abstract: Temperature microstructure casts are often analyzed to compute the diapycnal diffusivity K_ρ in geophysical flows. In the present study, we analyze 17 microstructure casts obtained during a Kelvin-Helmholtz billowing event at the base of the upper mixed layer in Lake Erie. From these casts, the turbulence properties of the mixing event are investigated and six parameterizations are applied to determine K_ρ. In comparison to the Osborn-Cox method, the four-equation overturn Froude number Fr_T vs. overturn Reynolds number Re_T parameterization and the four-equation buoyancy Reynolds number Re_b parameterization were found to be most accurate. Models with fixed mixing efficiency $\Gamma = 0.2$ performed poorly. From these data, we speculate that the transition to the Energetic Regime at high Re_b may occur when $Fr_T \sim 1$, giving $Re_b \sim Fr_T^2 Re_T \sim Re_T$.

1. Introduction: Kelvin-Helmholtz (KH) billows and other forms of shear instability drive vertical mixing of mass and momentum in stratified flows. These have been shown to vertically transport plankton (e.g., Pernica et al. 2013) and oxygen (e.g., Bouffard et al. 2013; 2014) in large lakes. In 2008-09 a large-scale field campaign was carried out in the central basin of Lake Erie with an objective to investigate the effects of physical processes on hypoxia in the lake. On July 22, 2008, (doy 204), when wind conditions were < 2 ms^{-1}, a series of 17 consecutive microstructure casts were obtained at approximately 10-min intervals at Sta. 341. Given the calm surface conditions (Fig. 1), we were surprised to observe large-scale (~2 m) KH billows at the base of the upper mixed layer (Fig. 2). Subsequent analysis (Bouffard et al. 2012) revealed that these were shear instabilities occurring at the crests and troughs of a progressive basin-scale internal Poincaré wave, which was energized by several days of mean daily winds ~7.5 ms^{-1} (Valipour et al 2015). Linear stability analysis revealed unstable modes with wavelengths ~9 m and periods ~400 s that agreed with the observed near-N peak in spectral density from thermistor chains (Bouffard et al. 2012). Here, the Brunt-Väisälä frequency $N = [(-g/\rho_o)(\partial\rho/\partial z)]^{1/2}$, where $\partial\rho/\partial z$ is the vertical density gradient and ρ_o = 1000 kgm^{-3} is a reference density. The objective of the present paper is to investigate the microstructure profiles to quantify the mixing and turbulence characteristics during the observed KH billow events.

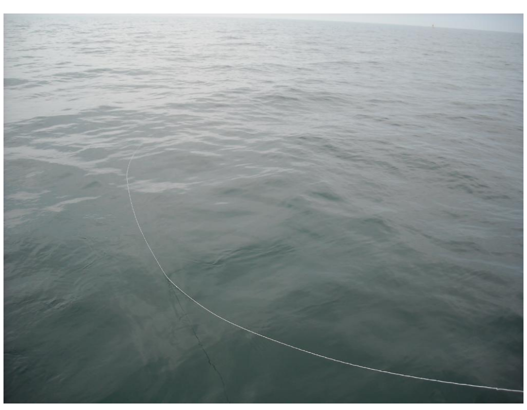

Figure 1: Typical field conditions during microstructure profiles on day 204 (17:10 h to 18:59 h GMT) at Sta. 341. Note calm free surface and absence of significant surface waves.

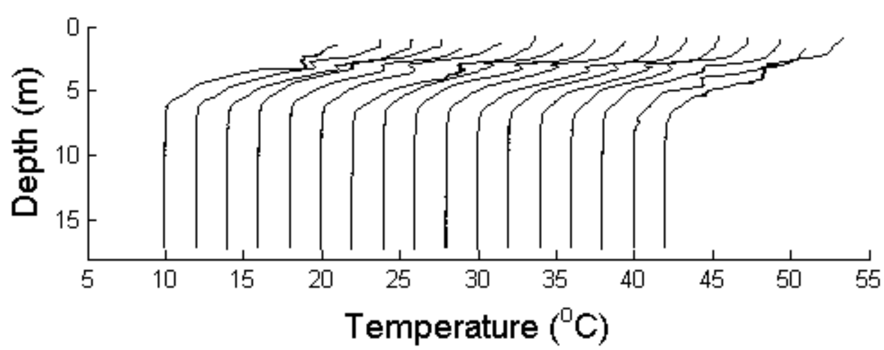

Figure 2: Microstructure temperature profiles recorded on day 204 (17:10 h to 18:59 h GMT) showing a succession of overturns located through the thermocline. Profiles were recorded at ~10-min intervals at the crest of the Poincare wave at Sta. 341 and, for clarity, are successively shifted by 2° C along the abscissa.

2. Methods: Microstructure casts were obtained from the Ontario Ministry of Natural Resources Keenosay on 22 July 2008 (day of year 204) at a central Lake Erie site (Sta. 341: N41°47′ W82°16′; ~50 km from shore and 18 m deep) using a Self Contained Autonomous Microstructure Profiler (SCAMP; Precision Measurement Engineering, www.pme.com). Profiling vertically through the water column at a speed of 0.1 m s^{-1} and with a sampling frequency of 100 Hz, the SCAMP resolved watercolumn temperature structure with vertical scales as small as 1 mm. Data were logged to two temperature gradient channels (T0 and T1) with T1 having a higher gain setting with a stronger signal-to-noise ratio. Unless otherwise noted, all data shown are from T1.

Individual casts were processed using MacSCAMP software (S. MacIntyre, pers. comm.), where the dissipation of turbulent kinetic energy ε was computed by fitting to the theoretical Batchelor spectrum (Ruddick et al. 2000). Turbulent diffusivity K_ρ was computed using several well known methods: (1) the rate of dissipation of temperature variance χ_T, where $K_\rho = \chi_T/(2\,(\partial T/\partial z)^2)$ (Osborn and Cox 1972, hereafter OC); (2) the rate of dissipation of turbulent kinetic energy ϵ, where $K_\rho = \Gamma\epsilon/N^2 = 0.2\epsilon/N^2$ and a typical value of Γ = 0.2 has been adopted (Osborn 1980, hereafter O20); (3) a two-equation overturn Froude number $Fr_T = (\epsilon/N^3 L_c^2)^{1/3}$ vs. overturn Reynolds number $Re_T = \epsilon^{1/3} L_c^{4/3}/\nu$ model (Ivey and Imberger 1991, hereafter II); (4) a four-equation Fr_T vs. Re_T model (Ivey et al. 1998, hereafter IIK); (5) the buoyancy Reynolds number $Re_b = \epsilon/\nu N^2$ (Barry et al. 2001; Shih et al. 2005; Bouffard and Boegman 2013, hereafter BSB); and (6) the Thorpe lengthscale L_T, where $K_\rho = 0.2 L_T^2 N$ (Thorpe 2005, hereafter LT).

Here, $\partial T/\partial z$ is the vertical gradient of the mean temperature profile, the lengthscale of the most energetic overturns is L_c and the mixing efficiency is defined in terms of the flux Reynolds number $\Gamma = R_f/(1 - R_f)$.

K_ρ from the OC model is taken as the benchmark (e.g., Dunckley et al. 2012), because it does not require estimation of a mixing efficiency; however, this model does require an assumption on the anisotropy of the flow (Ivey et al. 2008). Often, temperature microstructure data are not available and so K_ρ must be computed from thermistors and acoustic Doppler velocimeters and /or current profilers (e.g., Lorke 2007). In these instances, χ_T is not available, and so there remains a need to test the accuracy of other K_ρ parameterizations, relative to the benchmark OC method.

3. Results:

3.1 Flow field: The billows appear to be growing (Fig. 2; casts 2-6 and 8-14) between 2-6 m depth with large-scale ~1 m density inversions over an approximate timescale of ~1 h, or collapsing (casts 1, 7 and 15-17) with ~10 cm overturns over a ~1 m quasi-isothermal mixing region). In the upper mixed layer overturn events, and also through the weakly stratified hypolimnion where N becomes zero, L_T approached the Ozmidov scale and $Re_T \sim Re_b >> Fr_T$ (Fig. 3). These two regions of the water column differ in turbulence intensity (Fig. 3a,b), but are both neutrally stratified, with L_T , Re_T, Re_b and Fr_T being similar, causing these parameters to be insufficient for characterizing a turbulent billow event, relative to a weakly stratified hypolimnion (Fig. 3c-f). Only temperature gradient (not shown), ϵ and χ_T were elevated through only the billows (Fig. 3a,b). Shear regions at the base of surface layer may also be characterized by combinations of non-dimensional parameters (e.g., $0.8 < Fr_T < 3$ and $10 < Re_T < 4\text{x}10^3$; Imberger and Ivey 1991), which is consistent with our observations (not shown).

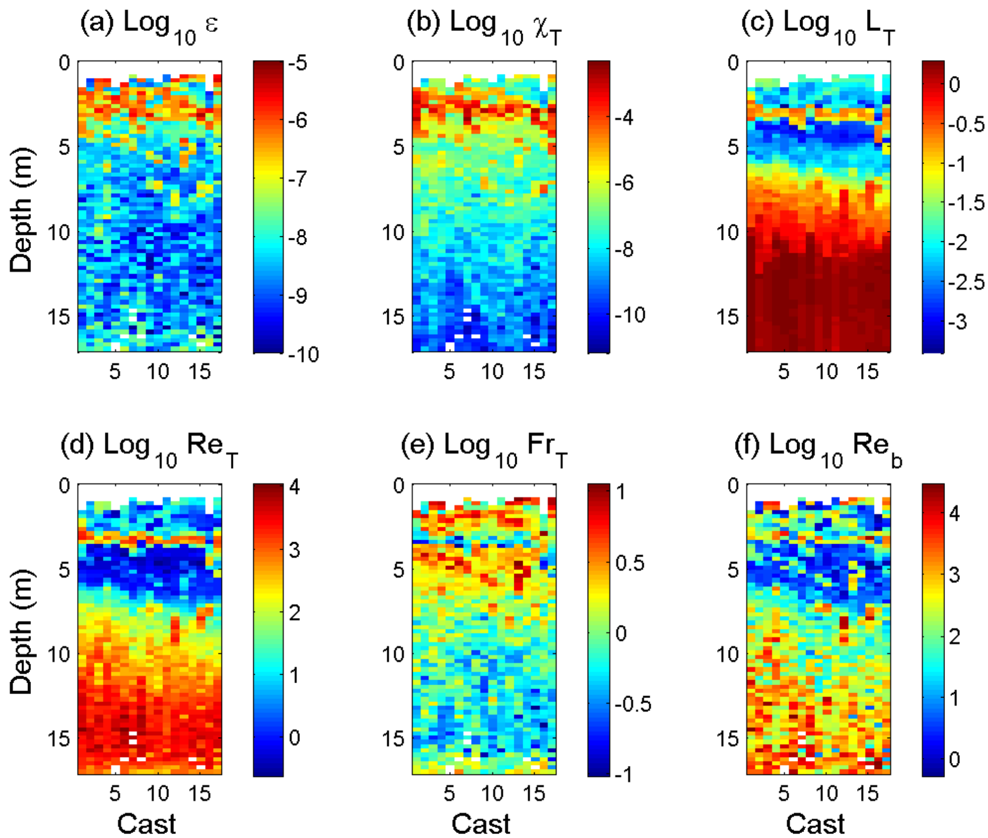

Figure 3: Contours of (a) turbulent dissipation, (b) temperature variance, (c) Thorpe overturn scale, (d) overturn Reynolds number, (e) overturn Froude number, and (f) buoyancy Reynolds number, computed form the 17 microstructure casts.

3.2 Application of turbulent diffusivity models:

We compare K_ρ from the six models as profiles (Fig. 4) and in Re_T vs. Fr_T space (Fig. 5). In general, the model results are within the same order of magnitude within the upper mixed layer and thermocline (Fig. 4), showing a K_ρ peak at the depth of the billows (~5m). The O20 model over-predicts mixing through the thermocline by a factor of 10, where mixing efficiency is likely reduced by the density stratification. In the hypolimnion, the OC and LT models give significantly lower and higher K_ρ (by a factor of 100), respectively, than the other models. IIK shows no variability through this region. The large spikes in K_ρ are expected when OC is used in well-mixed regions, such as the Lake Erie hypolimnion, due to small values of the mean temperature gradient in the denominator leading to poor estimates of χ_T (e.g., Dunckley et al. 2012).

In Re_T vs. Fr_T space, the OC model has a trend of increasing K_ρ with Re_T and with Fr_T at high Re_T (Fig. 5a). This models is not parameterized as a function of Fr_T or Re_T and shows more scatter than the others. From visual inspection, the two best models are IIK and BSB. As expected, the BSB model (Fig. 5b) gives increasing K_ρ with increasing Re_T and Fr_T (i.e., Re_b), whereas the IIK model (Fig. d) gives increasing K_ρ with increasing Re_T. Both trends are visually consistent with OC (Fig. 5a). The BSB model shows better prediction at high Re_T and low Fr_T, where the IIK over-predicts K_ρ.

Conversely, the IIK model is closer to OC at low Re_T, where BSB over-predicts K_ρ. The O20 and LT models have similar trends to BSB and IIK, respectively (Figs. 5e,f), but with constant $\Gamma = 0.2$, these models significantly over-estimate K_ρ by up to two orders of magnitude as Fr_T and Re_T increase and the other models suggest $\Gamma < 0.2$ (Fig. 6). The II parameterization does not produce K_ρ estimates for $Fr_T \leq 0.63$, where the model returns $R_f < 0$ (Fig. 5c); as a result, II is unsuitable for the present flow (see also Dunckley et al. 2012). The more recent Fr_T vs. Re_T based IIK parameterization provided improved estimation of K_ρ at low Fr_T, relative to II.

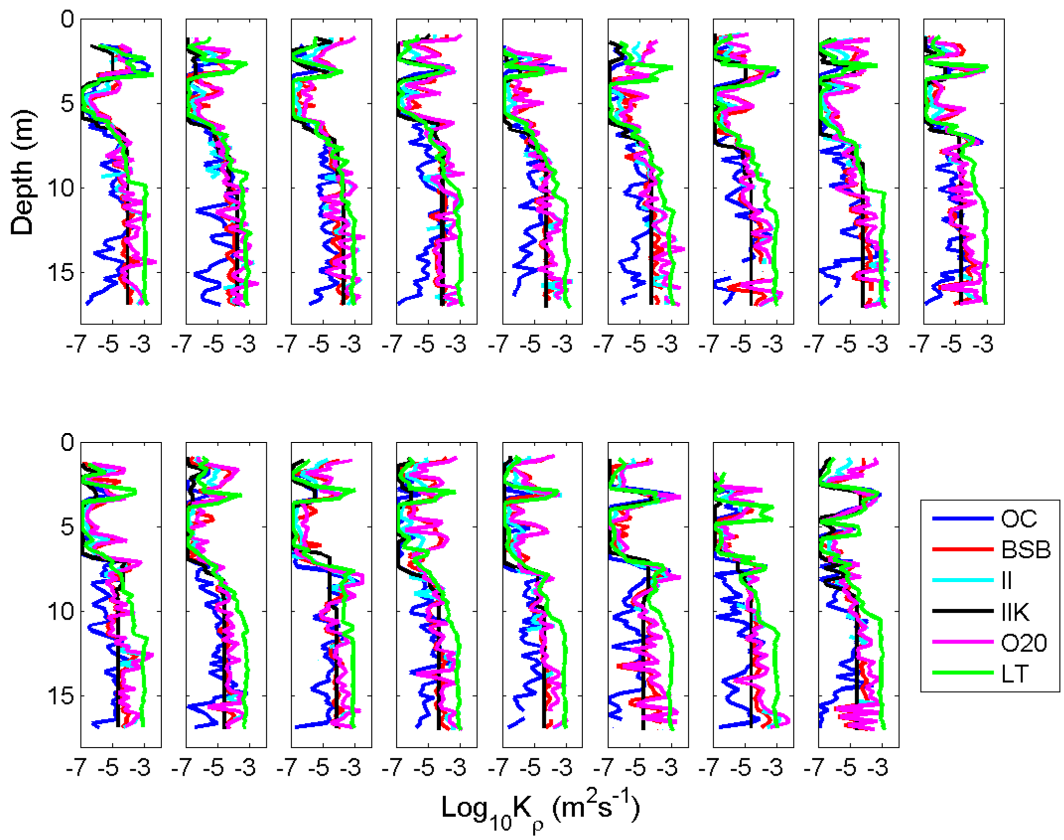

Figure 4: Profiles of turbulent diapycnal diffusivity for each of the 17 microstructure casts, computed using the six K_ρ parameterizations.

Table 1: Mean K_ρ values over all casts and bins for the various models. Root-mean-square (RMS) error of various K_ρ parameterizations in comparison to K_ρ computed with the Osborn-Cox model on temperature gradient channel T1 (OC_{T1}). Metrics for temperature gradient channel T0 (with lower gain) are also given.

Model	**K_ρ RMS Error vs. OC_{T1} (m^2s^{-1})**	**Mean K_ρ (m^2s^{-1})**
OC_{T1}	N/A	3.1×10^{-5}
OC_{T0}	4.2×10^{-5}	2.8×10^{-5}
BSB	1.3×10^{-4}	4.6×10^{-5}
II	4.3×10^{-4}	2.6×10^{-4}
IIK	1.4×10^{-4}	3.5×10^{-5}
LT	5.4×10^{-4}	3.7×10^{-4}

O20	5.4×10^{-4}	2.1×10^{-4}

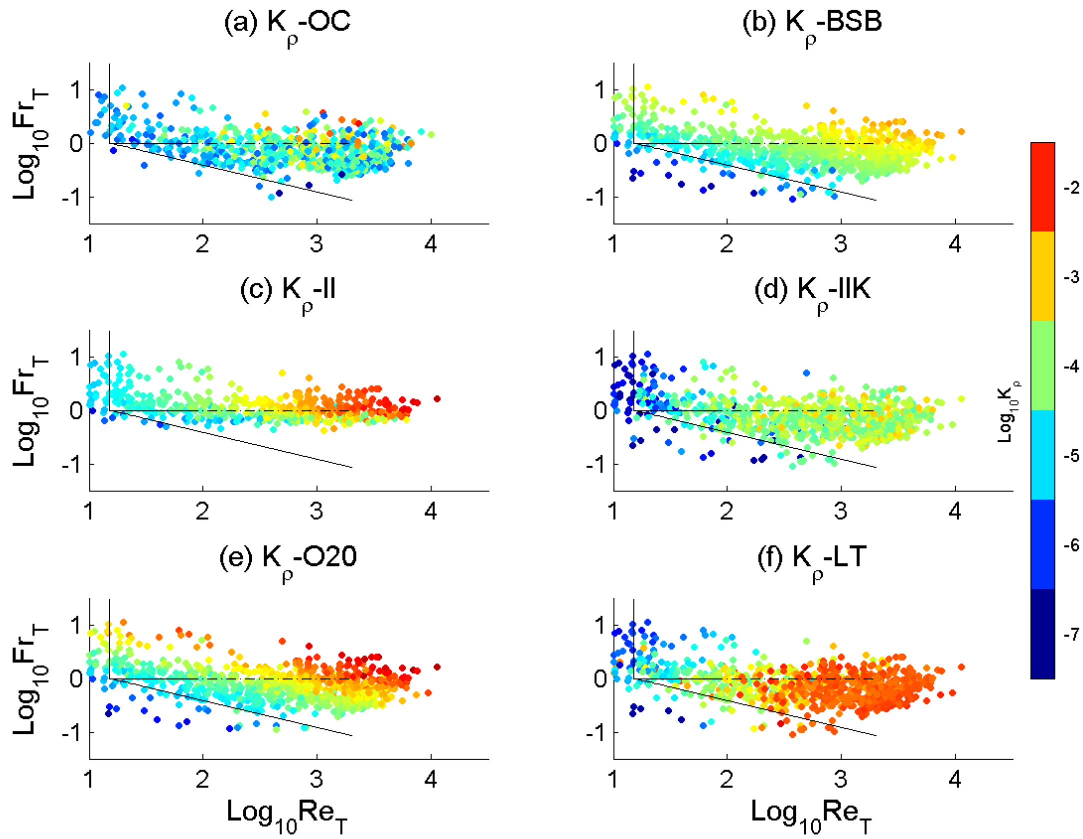

Figure 5: Scatter plot of K_ρ in Fr_T vs. Re_T space. Parameterizations include: (a) Osborn and Cox (1972), (b) Barry et al. (2001), Shih et al. (2005) and Bouffard and Boegman (2013), (c) Ivey and Imberger (1991), (d) Ivey, Imberger and Koseff (1998), (e) Osborn (1980) with Γ = 0.2, and (d) Thorpe (2005) with Γ = 0.2. The black lines denote turbulence regimes given in Ivey and Imberger (1991).

Mean K_ρ values (Table 1) from the OC method, IIK and BSB are similar (~10^{-5} m^2s^{-1}) and an order of magnitude smaller than from the II, LT and O20 models. The IIK model mean is closest to the OC, with a difference that is similar to the difference in means between the two temperature gradient channels. The K_ρ model RMS errors, relative to OC, are an order of magnitude larger than the error due to instrument gain (OC_{T0} in Table 1). As with the means, BSB and IIK have least error relative to OC.

In Fig. 6, we compare mixing efficiencies from II, IIK, BSB and OC. The later two models do not directly predict Γ, and so it is estimated by substituting for K_ρ into the Osborn (1980) model and solving for Γ. LT and O20 give Γ=0.2 throughout Re_T vs. Fr_T space and are not shown. BSB, IIK and II follow expected distributions, based on their parameterizations. The differences in these distributions are consistent with the associated differences in K_ρ predictions. For example, BSB over-predicts K_ρ at low Fr_T (Fig. 5b). In this region, BSB has a significantly higher mixing efficiency than the other models (~0.2 vs. ~0). Similarly, the over-prediction of K_ρ by IIK at over-predicts K_ρ at high Re_T and low Fr_T, where this model also gives high mixing efficiencies Γ ~ 0.2, relative to BSB and some OC data. The OC model shows significant scatter, yielding comparisons to the other models difficult.

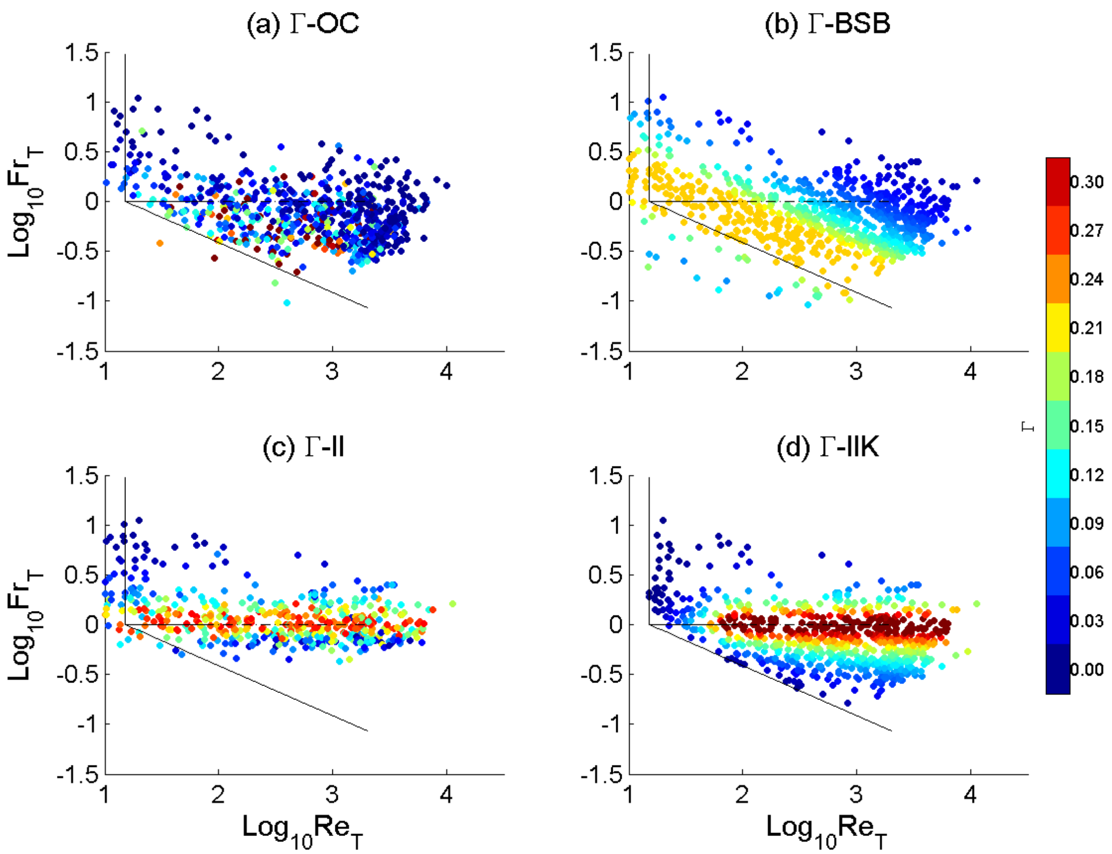

Figure 6: Scatter plot of Γ in Fr_T vs. Re_T space. Parameterizations include: (a) Osborn and Cox (1972), (b) Barry et al. (2001), Shih et al. (2005) and Bouffard and Boegman (2013), (c) Ivey and Imberger (1991), and (d) Ivey, Imberger and Koseff (1998). The mixing efficiency $\Gamma = 0.2$ throughout Fr_T vs. Re_T space for the Osborn (1980) and Thorpe (2005) models, and so is not shown. The black lines denote turbulence regimes given in Ivey and Imberger (1991).

4. Discussion and Conclusions:

We have investigated the turbulence characteristics of a mixing event in central Lake Erie and compared predictions of K_ρ during the event from six models. The BSB and IIK model predictions are closest to the OC model benchmark (lowest RMS error and closest mean, respectively). The II model is not suitable because it does not parameterize low Fr_T flows. The O20 and LT models over-predict K_ρ, on average by an order of magnitude, through not accounting for variable mixing efficiency.

We find the BSB and IIK models predict increasing K_ρ with increasing Re_T and Fr_T and increasing K_ρ with increasing Re_T, respectively. Both agree visually with OC. This is somewhat contrary to Dunckley et al. (2012), who show good prediction of OC by BSB throughout Re_T and Fr_T space. They did not have OC data at low Re_T and high Fr_T (Near Laminar regime; see Mater et al. 2014) and so did not observe the breakdown of the BSB model in this region, where the BSB mixing efficiency is not effectively parameterized. Under BSB, K_ρ is unable to default to the molecular value in this laminar region. Given the scatter in our OC data, we were not able to determine which trends in K_ρ and Γ are correct. Future work, to average turbulence quantities over Thorpe lengthscales and include analysis of the other ~600 SCAMP casts from Lake Erie and other sites may improve these results. Contributions of atmospheric data to this endeavour would be welcomed.

Some errors in Γ and consequently K_ρ may result from recently observed inconsistencies in the transition to lower Γ as Re_b increases (i.e., transition point to the Energetic Regime). In the lab-scale data used for the BSB parameterization, Γ begins to decrease at $Re_b \sim 100$. However, in lake and oceanic data, the transition occurs near $Re_b \sim 10^2$ - 10^3 (e.g., Bouffard and Boegman 2013, Walter et al 2014) and in the atmospheric boundary layer near $Re_b \sim 10^4$-10^5 (e.g., Mater et al 2014). High mixing efficiency, despite high Re_b, implies that geophysical flows occupy a high Re_T and Fr_T regime not achieved in the lab and DNS (Mater et al 2014).

Insight on the Re_b transition to energetic turbulence with low Γ as Re_b increases may be obtained from Ivey and Imberger (1991; their Fig 2) and Mater et al. (2014; their Fig. 2). They show that for $Fr_T > 1$, the turbulence becomes energetic with a well-developed velocity spectrum and mixing resulting from near Kolmogorov-scale L_k overturns. The normalized buoyancy flux tends to an asymptotic value and as Fr_T increases, and Γ tends to zero. This suggests the transition to energetic turbulence, with lower Γ, occurs at $Fr_T \sim 1$, giving $Re_b \sim Fr_T^2 Re_T \sim Re_T$ (Fig. 7). There is too much scatter in our Γ data to test this transition point; however, this argument is consistent with the differences between models in the present study, which occur along the Re_T axis. Similarly, Bluteau et al. (2013) hypothesized the higher Γ transition for published atmospheric data might be caused by larger Re_T, and observed an increase in Γ with increasing Re_T at an energetic oceanic site. We may also define $Re_T = (L_c/L_k)^{4/3}$ as a measure of the bandwidth of eddy cascade that will increase with Reynolds number of the flow, from lab to atmosphere (Tennekes and Lumley 1972; their Fig. 8.7).

Alternative approaches to compute K_ρ and Γ that include the gradient Richardson number Ri_g have been proposed from Direct Numerical Simulations; however, the high resolution velocity data required to compute Ri_g (e.g., Mater et al. 2104) within the thin ~10 cm shear layers often observed in the field (e.g., Boegman et al. 2003) is typically not available.

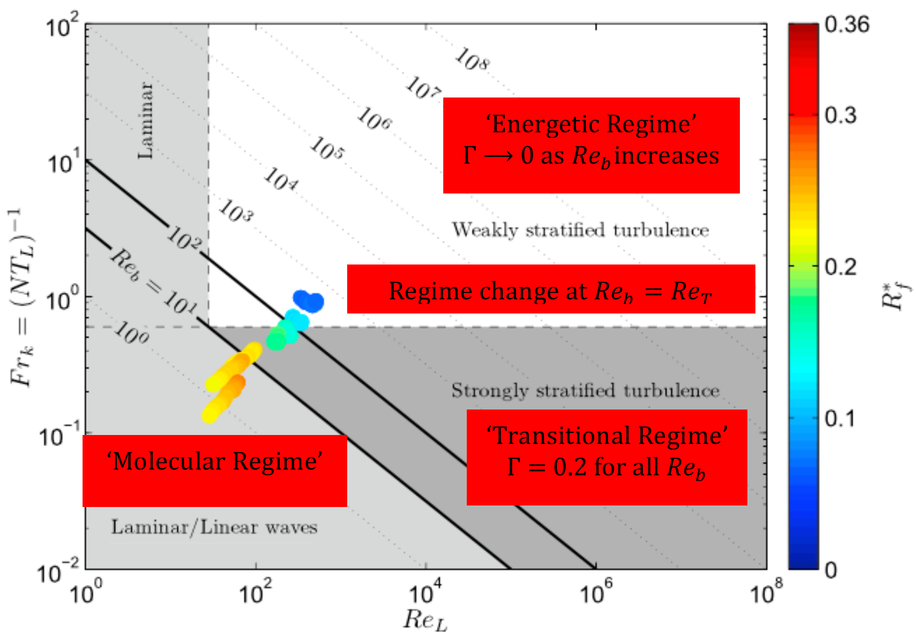

Figure 7: Parameter space for interpretation of turbulence in Fr_T (Fr_k) vs. Re_T(Re_L) space. Reproduced from Mater et al. (2014). R_f data are from Shih et al. (2005). Regime lines are approximations. Red boxes show proposed change in regime at $Re_b = Re_T$ (i.e., $Fr_T \sim 1$). The regime change occurs at $Re_b \sim 100$ for lab-scale data (shown), $Re_b \sim 10^3$ for lake/oceanic data (e.g., Bouffard and Boegman 2013, Walter et al 2014) and $Re_b \sim 10^5$ for atmospheric data (e.g., Mater et al 2014).

Acknowledgements: This research was funded by an NSERC Strategic Grant to J.D. Ackerman, L. Boegman, K.G. Lamb (PI), and R.E.H. Smith. The authors are indebted to Yerubandi R. Rao and R. Valipour (National Water Research Institute) for providing some data and logistical help and S. MacIntyre for providing SCAMP processing routines. We thank the crew of the Keenosay for their help in the field. Environment Canada and the Ontario Ministry of Natural Resources provided ship time. The SCAMP was purchased with CFI/IOF grants to LB.

5. References:

Barry, M.E., Ivey, G.N., Winters, K.B. and Imberger, J., 2001. Measurements of diapycnal diffusivities in stratified fluids. *Journal of Fluid Mechanics*, *442*, pp.267-291.

Bluteau, C.E., Jones, N.L. and Ivey, G.N., 2013. Turbulent mixing efficiency at an energetic ocean site. *Journal of Geophysical Research: Oceans*,*118*(9), pp.4662-4672.

Boegman, L., Imberger, J., Ivey, G.N. and Antenucci, J.P., 2003. High-frequency internal waves in large stratified lakes. *Limnology and Oceanography*, *48*(2), pp.895-919.

Bouffard, D., Ackerman, J.D. and Boegman, L., 2013. Factors affecting the development and dynamics of hypoxia in a large shallow stratified lake: hourly to seasonal patterns. *Water Resources Research*, *49*(5), pp.2380-2394.

Bouffard, D., Boegman, L. and Rao, Y.R., 2012. Poincaré wave-induced mixing in a large lake. *Limnology and Oceanography*, *57*(4), p.1201

Bouffard, D. and Boegman, L., 2013. A diapycnal diffusivity model for stratified environmental flows. *Dynamics of Atmospheres and Oceans*, *61*, pp.14-34.

Dunckley, J.F., Koseff, J.R., Steinbuck, J.V., Monismith, S.G. and Genin, A., 2012. Comparison of mixing efficiency and vertical diffusivity models from temperature microstructure. *Journal of Geophysical Research: Oceans*,*117*(C10).

Imberger, J. and Ivey, G.N., 1991. On the nature of turbulence in a stratified fluid. Part II: Application to lakes. *Journal of Physical Oceanography*, *21*(5), pp.659-680.

Ivey, G.N. and Imberger, J., 1991. On the nature of turbulence in a stratified fluid. Part I: The energetics of mixing. *Journal of Physical Oceanography*,*21*(5), pp.650-658.

Ivey, G.N., Imberger, J. and Koseff, J.R., 1998. Buoyancy fluxes in a stratified fluid. *Physical Processes in Lakes and Oceans*, pp.377-388.

Ivey, G.N., Winters, K.B. and Koseff, J.R., 2008. Density stratification, turbulence, but how much mixing? *Annual Review of Fluid Mechanics*, *40*(1), p.169.

Lorke, A., 2007. Boundary mixing in the thermocline of a large lake. *J. Geophys. Res.*, *112*(C9).

Mater, B.D. and Venayagamoorthy, S.K., 2014. The quest for an unambiguous parameterization of mixing efficiency in stably stratified geophysical flows. *Geophys. Res. Lett.*, *41*(13), pp.4646-4653.

Osborn, T.R., 1980. Estimates of the local rate of vertical diffusion from dissipation measurements. *Journal of Physical Oceanography*, *10*(1), pp.83-89.

Osborn, T.R. and Cox, C.S., 1972. Oceanic fine structure. *Geophy. Astrophys. Fluid Dyn.*, *3*, pp.321-345.

Pernica, P., Wells, M.G. and Sprules, W.G., 2013. Internal waves and mixing in the epilimnion of a lake affects spatial patterns of zooplankton in a body-size dependent manner. *Limnology and Oceanography: Fluids and Environments*, *3*(1), pp.279-294.

Ruddick, B., Anis, A. and Thompson, K., 2000. Maximum likelihood spectral fitting: The Batchelor spectrum. *Journal of Atmospheric and Oceanic Technology*, *17*(11), pp.1541-1555.

Shih, L.H., Koseff, J.R., Ivey, G.N. and Ferziger, J.H., 2005. Parameterization of turbulent fluxes and scales using homogeneous sheared stably stratified turbulence simulations. *J. Fluid Mech.*, *525*, pp.193-214.

Tennekes, H. and Lumley, J.L., 1972. *A first course in turbulence*. MIT press.

Thorpe, S.A., 2005. *The turbulent ocean*. Cambridge University Press.

Valipour, R., Bouffard, D., Boegman, L. and Rao, Y.R., 2015. Near-inertial waves in Lake Erie. *Limnology and Oceanography*, *60*(5), pp.1522-1535.

Walter, R.K., Squibb, M.E., Woodson, C.B., Koseff, J.R. and Monismith, S.G., 2014. Stratified turbulence in the nearshore coastal ocean: Dynamics and evolution in the presence of internal bores. *Journal of Geophysical Research: Oceans*, *119*(12), pp.8709-8730.